Comparative Biochemistry and Physiology, Part A 308 (2025) 111914

Contents lists available at ScienceDirect

Comparative Biochemistry and Physiology, Part A

journal homepage: www.elsevier.com/locate/cbpa

Research Article

Identification and functional characterization of a novel ovarian-specific Kelch domain-containing gene involved in the ecdysteroid signaling pathway of *Penaeus monodon*

Jakkapong Kluebsoongnoen [a,b,c], Duangrudee Tanramluk [a,d], Maryam Jozghorbani [b], Jutarop Phetcharaburanin [c,e], Tomasz J. Sarnowski [b,*], Apinunt Udomkit [a,*]

[a] Institute of Molecular Biosciences, Mahidol University, Salaya Campus, Nakhon Pathom, Thailand
[b] Institute of Biochemistry and Biophysics, Polish Academy of Sciences, Warsaw, Poland
[c] National Phenome Institute, Regional Science Park Northeast 1, Khon Kaen University, Khon Kaen, Thailand
[d] Integrative Computational BioScience (ICBS) Center, Mahidol University, Salaya Campus, Nakhon Pathom, Thailand
[e] Department of Systems Biosciences and Computational Medicine, Faculty of Medicine, Khon Kaen University, Khon Kaen, Thailand

ARTICLE INFO

Editor: Dr. Michael Hedrick

Keywords:
Ecdysone receptor
Kelch-containing protein
Shrimp

ABSTRACT

In crustaceans, vitellogenin (Vg) synthesis is regulated by complex hormonal and molecular networks. This study investigates the role of the ecdysone receptor (PmEcR) in regulating *Vg* expression and identifies downstream effectors in *Penaeus monodon*. Silencing of *PmEcR* using RNA interference resulted in a two-fold increase in *Vg* expression and a significant rise in the gonadosomatic index (GSI), suggesting *PmEcR* acts as a suppressor of vitellogenesis. Through a suppression subtractive hybridization (SSH) technique, an uncharacterized *LOC 113805388* gene, was identified as being downregulated upon *PmEcR* silencing. Functional and structural characterization revealed this transcript as an ovarian-specific protein with a β-propeller structure (Kelch-like domain-containing protein; PmKel), suggesting that it belongs to a Kelch-like protein family generally involved in protein-protein interactions in cellular regulation. LC-MS/MS analysis of the ovarian proteome confirmed the presence of the PmKel protein, verifying its expression in the ovary. *PmKel* expression displayed an inverse pattern to that of *Vg* during ovarian development, and its knockdown was associated with increased *Vg* transcript levels, suggesting a possible role in the regulation of *Vg* gene expression. In addition, a recombinant PmKel protein was produced and used as a bait to identify its partners in ovarian nuclear extract by affinity purification mass spectrometry (AP-MS). The isolated set of interacting proteins highlighted functional enrichment in mRNA and protein metabolic processes involved in developmental pathways. Also, these proteins could interact with a Kelch-like domain predicted on PmKel 3D protein structure by protein network analysis and protein-protein docking. These findings suggest that PmKel is a novel ovarian specific Kelch-containing protein that plays a key role in the vitellogenesis regulatory network via the EcR pathway. Collectively, these results add to the current knowledge of shrimp reproduction and may suggest future direction for improving reproductive performance in aquaculture.

1. Introduction

Shrimp reproduction is vital for the success and sustainability of aquaculture, as it directly influences productivity. Efficient reproduction ensures healthy broodstock and high yields, which are critical for meeting global demand. In crustaceans, ovarian development is regulated by complex physiological processes, including nutritional accumulation, body development, and hormonal control. Notably, endocrine regulation plays a key role in timely vitellogenesis, which is divided into synthesis and accumulation of vitellogenin (Vg), a yolk protein precursor essential for oocyte maturation (Tsukimura, 2001). Understanding the hormonal mechanisms behind these processes can provide strategies to optimize reproductive performance and thus, enhance the efficiency of shrimp farming.

The X-organ/sinus gland (XO/SG) neurosecretory system plays a central role in controlling vitellogenesis. The crustacean hyperglycemic

* Corresponding author.
E-mail addresses: tsarn@ibb.waw.pl (T.J. Sarnowski), apinunt.udo@mahidol.ac.th (A. Udomkit).

https://doi.org/10.1016/j.cbpa.2025.111914
Received 10 March 2025; Received in revised form 29 July 2025; Accepted 30 July 2025
Available online 31 July 2025

hormone super-family (CHHs) is a well-known master regulator controlling growth and reproduction in crustaceans (Webster et al., 2012). A gonad-inhibiting hormone (GIH) is characterized in the CHH class II subfamily, and plays a distinct role in hindering gonad maturation (Treerattrakool et al., 2008). Other hormones belonging to CHH class II include molt-inhibiting hormone (MIH) and mandibular organ-inhibiting hormone (MOIH) (Zmora et al., 2009; Ding et al., 2023). The GIH is released into the hemolymph and acts on the hepatopancreas and ovary to target vitellogenesis. Alongside these peptides, lipophilic and steroid hormones, methyl farnesoate (MF) and ecdysteroids play essential roles in modulating vitellogenesis (Subramoniam, 2000; Nagaraju, 2011). These hormones, which are often under the regulatory influence of CHH Class II peptides, are recognized as critical stimulants for reproductive, molting, and developmental processes in crustaceans. Together, the coordinated actions of these hormonal factors ensure the precise timing and progression of vitellogenesis, supporting successful reproduction in crustaceans.

The ecdysone signaling pathway is a critical regulator of molting, reproduction, and development in arthropods. In this pathway, ecdysteroids synthesized in the Y-organs are converted into 20-hydroxyecdysone (20E) and transported via the hemolymph to target tissues, where it binds to the ecdysone receptor (EcR) and its heterodimeric partner, ultraspiracle protein (USP) or its homolog retinoid-X receptor (RXR), forming a transcriptional complex that modulates gene expression (Costantino et al., 2008). The *Vg* gene is one of the well-established targets of EcR, directly linking ecdysone signaling to oocyte maturation and ovarian development. For instance, *EcR* silencing in a mud crab *Scylla paramamosain* suppressed *Vg* expression in the ovary, demonstrating a positive regulatory role for *EcR* in *Vg* synthesis (Gong et al., 2015). However, exogenous estrogen stimulation in *Portunus trituberculatus* increased *Vg* expression without significantly affecting *EcR*, *RXR*, or estrogen-related receptor (*ERR*) expression in the ovary or hepatopancreas, highlighting potential differences in regulatory pathways of *Vg* expression (Lu et al., 2018). Additionally, RXR has been shown to regulate *Vg* expression independently of ecdysone signaling (Gong et al., 2016; Kluebsoongnoen et al., 2021). Hence, crustacean's ecdysone signaling pathway requires further investigation to clarify its contributions in reproductive processes.

In this study, we investigated genes that potentially take part in EcR-mediated *Vg* expression in *Penaeus monodon* (*P. monodon*) ovaries. Suppression subtractive hybridization (SSH) following *EcR* silencing by RNAi led to the discovery of a novel gene potentially involved in regulating *Vg* called by us *PmKel*. Structural and functional characterization as well as protein interactome analysis of the PmKel protein described in this study will contribute to a deeper understanding of the molecular mechanisms underlying vitellogenesis in crustaceans through the ecdysteroid signaling pathway and offer potential applications for improving captive reproduction in shrimp aquaculture.

2. Materials and methods

2.1. Shrimp preparation

Female shrimp *P. monodon*, at vitellogenic stages (~250 g), were caught from the Gulf of Thailand, Chonburi Province, Thailand. Immature female shrimp (~50 g), were domesticated shrimp kindly provided by the Shrimp Genetic Improvement Center, Surat Thani, Thailand. The information regarding molting and ovarian stages of the experimental shrimp were described in Table S1. The shrimps were cultured in 30 ppt seawater at 28 °C during the 2–3 weeks experimental period at the Center of Applied Shrimp Research and Innovation, Institute of Molecular Biosciences, Mahidol University. All the animal experiments were done in accordance with the Animal Care and Use Protocol of the Mahidol University-Institute Animal Care and Use Committee (MU-IACUC).

2.2. In vivo PmEcR silencing

To validate *EcR* suppression in shrimp ovaries, *EcR*-dsRNA was synthesized in *Escherichia coli* and was injected into mature female *P. monodon* at 2.5 $\mu g.g^{-1}$ shrimp body weight, with NaCl-treated shrimp serving as a control as described earlier (Kluebsoongnoen et al., 2023). At day 10 post-injection (dpi), the total RNA was extracted from shrimp ovaries using TRIzol Reagent (Invitrogen, USA) following the manufacturer's protocol. First-strand cDNA was synthesized from 2 μg of total RNA using PRT-oligo-dT16 primers and Improm II™ reverse transcriptase (Promega, USA) under the following conditions: 25 °C for 5 min, 42 °C for 60 min, and 70 °C for 15 min. PCR amplification of *EcR* and *Vg* transcripts was performed in 25 μl reactions containing 1 μl cDNA, 0.2 μM of gene-specific primers, 0.2 mM dNTPs, 1× Taq buffer, and 1.25 U Taq DNA polymerase (New England BioLabs, USA). The PCR conditions for *EcR* and *Vg* were as follows: 94 °C for 2 min; 35 cycles of 94 °C for 15 s, 55 °C for 15 s, 68 °C for 2 min; and a final extension at 72 °C for 3 min. *Actin* (internal control) was amplified in a separate reaction using actin-F and actin-R primers under the following conditions: 94 °C for 2 min; 21 cycles of 94 °C for 30 s, 55 °C for 30 s, 74 °C for 1 min; and a final extension at 74 °C for 7 min. Amplicons of either *EcR* (772 bp) or *Vg* (380 bp) were electrophoresed on the same 1.2 % agarose gels as *actin* (550 bp) and quantified using ImageJ software version 1.54 k (Schneider et al., 2012). All the used primers were listed in Table 1.

2.3. Suppression subtractive hybridization (SSH) library construction

To investigate differentially expressed genes (DEG) under *PmEcR* silencing by SSH, poly A^+ RNA was isolated from 1 mg of pooled total RNA of *EcR*-dsRNA-treated or NaCl-treated shrimp ($n = 3$ each) using the Poly A^+ Spin™ mRNA Isolation Kit (New England Biolabs, USA). A total of 1.5 μg of poly A^+ RNA from each group was used to construct forward and reverse SSH libraries with the PCR™ cDNA Subtraction Kit (Clontech, USA). In the forward library, cDNA from the *EcR*-knockdown group served as the tester, while the control group cDNA was the driver to identify upregulated genes. For the reverse library, the roles of cDNA from both groups were reversed to detect downregulated genes. The efficiency of SSH was validated by *Actin* amplification, and nested PCR products were analyzed on 1.2 % agarose gels. Differentially amplified bands were subcloned into the pGEM-T Easy vector (Promega, USA) then, transformed into *E. coli* DH5α and screened by *Eco*RI restriction digestion. Subtracted library sequences were submitted for automated DNA sequencing at 1st BASE Laboratories (Malaysia), trimmed using BioEdit, and annotated by sequence homology searches with BLASTn and BLASTx (NCBI GenBank). Matches with *E*-values $<1 \times 10^{-7}$ were considered significant. The expressions of these observed sequenced bands, including *Thrombospondin II* (*TSP II*), *peritrophine I (Per I), uncharacterized LOC 113805388*, *Pole hole-like protein*, and *Nebulin anchoring protein (NRAP)* were quantified using RT-qPCR with *EF-1α* as an internal control. The reaction mixture contained SYBR® Green (KAPABIOSYSTEMS, USA) and 0.2 pmol of qKel-F and qKel-R primers, with amplification carried out on an ABI® Prism 7500 system. The thermal profile was 95 °C for 3 min, followed by 40 cycles of 95 °C for 5 s and 60 °C for 30 s. Relative transcript levels were calculated using the $2^{-\Delta\Delta Ct}$ method (Livak and Schmittgen, 2001).

2.4. PmKel cloning and protein 3D structure prediction

This study focused on a ~ 1 kb fragment of the uncharacterized *LOC 113805388* gene obtained from the reverse SSH library. The cloning of this cDNA was performed by extracting total RNA from shrimp ovaries using Trizol Reagent (Invitrogen, USA), followed by first-strand cDNA synthesis as previously described. To clone the full-length cDNA, specific primers were designed based on the partial sequence of the uncharacterized *LOC 113805388* gene. For 3′ RACE, 0.2 μM each of an internal forward primer (Unc-F1) and the PRT primer were used to amplify the 3′

Table 1
Primer used in this study.

Primer	Sequences (5′- > 3′)	Experiment
PRT	CCGGAATTCAAGCTTCTAGAGGATCCTTTTTTTTTTTTTTTT	
3EcR-F	CTTAAGTCCTGTGCCACAAACC	
EcR-R	TTATTTAGGTGTGACGTCCCATATC	
Unc-F	GTCTAACTAGCACCAGTGGTG	
Unc-R	GCTGCTGAAGCTGTAGACATG	cDNA synthesis and genes expression
Vg-F1	CTAAGGCAATTATCACTGCTGCT	
Vg-R1	AAGCTTGGCAATGTATTCCTTTT	
Actin-F	GACTCGTACGTCGGGCGACGAG	
Actin-R	AGCAGCGGTGGTCATCACCTGCTC	
PM-1	CCGGAATTCAAGCTTCTAGAGGATCC	
Unc-R1	GCTGCTGAAGCTGTAGACATG	
Unc-R2	GGCATCATCTCCTGTCCTG	
Unc-R3	CAAGTAGAACTGCTCTAGTCAT	
Unc-F1	GTCTAACTAGCACCAGTGGTG	RACE and cloning
Unc-F2	GTTGTAACGGGTGAGACTGG	
PmKel-F	ATGAGGGGTGCCATGACAGG	
PmKel-R	TCACACTGGGACTATTGGC	
qKel-F	GCACCAGTGGTGAGATTGGAGATG	
qKel-R	GCCATCCACTGGGTGGCTAG	
qVg-F	CCATCTGCAGCACCAATCTTCGC	
qVg-R	GCAACAGCCTTCATTCTGATGCCA	
qTSP-F	GGCAGCACTGCTTTGGCATGA	
qTSP-R	ACCCTGGTACAAGTAGAACCTAATGG	
qPer1-F	GCTTGGTGGCGTGTTGCAG	
qPer1-R	GGCCTGGACACAAGTTATCAGGG	qPCR
qPole-F	TCCCCCATCAGTATTGAACC	
qPole-R	GCCACAGGCAAGAGCTTTGG	
qNRAP-F	GATCGAGGTGCCCACAGGA	
qNRAP-R	CGGCAGGATAAACCCCATACCC	
qEcR-F	GCTGCACGTCGTTATGACGC	
qEcR-R	GCCTCACGGAGGAATGGTCG	
qEF1α-F	GAACTGCTGACCAAGATCGACAGG	
qEF1α-R	GAGCATACTGTTGGAAGGTCTCCA	
SLKel-F	GCTCTAGAGCGGCTGTAATCACTGCT	
SLKel-R	CGGAATTCCTATTTGTCCTGCTGCAGC	Kel-dsRNA construction
STKel-F	CGCTCGAGGCGGCTGTAATCACTGCT	
STKel-R	CGGAATTCGTCTGCACCAGAGCCAAC	
KelGH-F	CGGAATTCATGAGGGGTGCCATGACAGG	rKel protein construction
KelGH-R	GCGTCGACTCAGTGGTGGTGGTGGTGCACTGGGACTATTGGC	

UTR from 1 μl of the first-strand cDNA, with 1.25 U Taq DNA polymerase (New England BioLab, USA). The reaction was subjected to 94 °C for 2 min, followed by 35 cycles of 94 °C for 15 s, 50 °C for 15 s, and 68 °C for 2 min, with a final extension at 72 °C for 3 min. A nested PCR was performed using Unc-F2 and PM1 primers to obtain specific amplification.

For 5′ RACE, first-strand cDNA synthesis was performed using Unc-R1 instead of the PRT primer. The resulting cDNA was polyadenylated with 200 μM dATP, 1× TdT buffer, and 20 U of TdT (Thermo Fisher Scientific, USA) in a 30 μl reaction, incubated at 37 °C for 20 min, and heat-inactivated at 65 °C for 10 min. The first-round PCR was carried out using 3 μl of dA-tailed cDNA, Unc-R2, and PRT primers under the same conditions as 3′ RACE. A second-round PCR with Unc-R3 and PM1 primers was performed to obtain specific products. Amplified bands from 3′ and 5′ RACE were subcloned and sequenced, and the full open reading frame (ORF) was identified using the NCBI ORF Finder.

The deduced amino acid sequence of an uncharacterized LOC 113805388 was analyzed using AlphaFold (Jumper et al., 2021) to predict the 3D protein structure. The top-ranking model, based on predicted Local Distance Difference Test (pLDDT) scores, was selected and visualized using ChimeraX (Pettersen et al., 2021) to inspect the overall fold and functional residues. Structural domains were identified by uploading the PDB file to the Vector Alignment Search Tool (VAST). Based on the presence of a Kelch-like containing domain at the C-terminus on 3D structure, this protein was renamed to PmKel.

2.5. Transcriptional profile of PmKel

To analyze tissue-specific expression, total RNA extraction and cDNA synthesis were performed as previously described. Shrimp tissues including brain, eyestalk, thoracic ganglion, abdominal ganglion, heart, muscle, gill, hepatopancreas, lymphoid organ, and ovary were collected from female shrimp at vitellogenic stage. The *PmKel* transcript was detected using semi-quantitative RT-PCR in a 25 μl reaction containing 1 μl of first-strand cDNA, 0.2 μM each of Unc-F and Unc-R primers, 0.5 mM dNTPs, 1× Taq buffer, 1.25 U Taq DNA polymerase (New England BioLabs, USA), and distilled water. PCR conditions were as follows: 94 °C for 2 min; 25 cycles of 94 °C for 15 s, 55 °C for 15 s, 68 °C for 2 min; followed by a final extension at 72 °C for 3 min. *Actin* was amplified as an internal control using PmActin-F and PmActin-R primers under the following conditions: 21 cycles of 94 °C for 30 s, 55 °C for 30 s, 74 °C for 1 min, with a final extension at 74 °C for 7 min.

To examine *PmKel* expression during ovarian maturation, ovaries were categorized into five stages based on the gonadosomatic index; GSI (Tan-fermin and Pudadera, 1989). Total RNA extraction and cDNA synthesis were performed as described above. The expression levels of *PmKel* as well as *EcR, and Vg* were quantified using RT-qPCR with *EF-1α* as an internal control as described previously.

2.6. PmKel-dsRNA construction

A 500 bp stem-loop fragment of *PmKel*-dsRNA, targeting the middle region of the ORF (+1264 to +1763 bp), was designed and produced

using a bacterial expression system. The DNA template for the stem-loop fragment was amplified with primers SLKelF and SLKelR, while the stem template fragment (420 bp) was amplified with primers STKelF and STKelR. The stem-loop fragment was cloned into pET17b vector at the *Xba*I and *Nco*I sites, followed by cloning of the stem fragment at the *Xho*I and *Nco*I sites. The recombinant Kel-pET17b plasmid was transformed into *E. coli* DH5α for sequence verification and then, re-transformed into *E. coli* HT115 for expression. Specific stem-loop dsRNA targeting *PmKel* was expressed by inducing with 0.4 mM IPTG in 2×YT medium for 4 h at 37 °C with shaking. The dsRNA was extracted using Trizol Reagent (Invitrogen, USA), dissolved in 150 mM NaCl, and stored at −30 °C until use. Concentration and purity of dsRNA were assessed by agarose gel electrophoresis, and the quality was verified by RNase digestion assay.

2.7. In vivo silencing of PmKel

Vitellogenic female shrimp (~250 g) were divided into three groups: negative control injected with NaCl, non-specific control injected with *GFP*-dsRNA (2.5 μg.g^{-1} body weight), and experimental group injected with *PmKel*-dsRNA (2.5 μg.g^{-1} body weight). At 10 dpi, the ovaries were dissected, total RNA was extracted, and the first-strand cDNA was synthesized as described above. Suppression of *PmKel* and *Vg* expressions in ovarian tissues was quantified using RT-qPCR.

2.8. Production of recombinant Kel/GST-6×His fusion protein

The DNA fragment encoding the mature peptide of *PmKel* was amplified by PCR using the *PmKel* plasmid as a template. The 25 μl reaction contained 10 ng plasmid, 0.2 mM dNTPs, 1× Q5 buffer, 1× Q5 GC-rich buffer, 0.5 μM each of KelGH-F and KelGH-R primers, 0.02 U Q5 DNA polymerase (New England BioLabs, USA). PCR conditions were: 94 °C for 2 min, followed by 35 cycles of 94 °C for 15 s, 50 °C for 15 s, and 72 °C for 2 min, with a final extension at 72 °C for 3 min. The amplified product was digested with *Eco*RI and *Sal*I, ligated into the pGEX4T-1 vector, and transformed into *E. coli* DH5α for sequencing verification (Institute of Biochemistry and Biophysics, Polish Academy of Sciences, Poland). The confirmed plasmid was re-transformed into *E. coli* BL21 Sol cells for protein expression.

To produce a recombinant Kel/GST-6×His fusion protein (rPmKel/GST-6×His), a single colony of *E. coli* BL21 Sol containing the recombinant plasmid (Kel/GST-6×His) or the control plasmid (GST-6×His) was inoculated into 10 ml LB broth supplemented with 100 μg/ml ampicillin and 34 μg/ml chloramphenicol. Cultures were incubated overnight at 37 °C and diluted 1:50 in fresh LB containing the same antibiotics. Cells were grown at 37 °C until OD_{600} reached 0.6–1.0 then, induced with 1.0 mM IPTG, and incubated for 3 h. The cells were harvested by centrifugation at 6000 rpm for 15 min at 4 °C, and the pellets were resuspended in lysis buffer (50 mM phosphate buffer pH 8.0, 0.3 M NaCl, 5 mM $MgCl_2$, 10 % glycerol, 1 % Triton X-100, 25 mM imidazole, 5 mM β-mercaptoethanol, 1 mM PMSF, 1 μg/ml DNase, 0.1 mg/ml lysozyme, 1× protease inhibitor cocktail). The lysate was incubated overnight at −20 °C, disrupted using a French press, and analyzed on 10 % SDS-PAGE.

For protein purification, the insoluble fraction was solubilized in buffer B (100 mM NaH_2PO_4, 10 mM Tris-Cl, 8 M urea, pH 8.0) on ice for 30 min, followed by centrifugation at maximum speed for 10 min at 4 °C. The supernatant was diluted 10-fold with binding buffer (50 mM phosphate buffer pH 8.0, 0.3 M NaCl, 10 % glycerol, 25 mM imidazole, 1 mM PMSF, 1× protease inhibitor cocktail) to remove urea using a 30 K Amicon® Ultra filter (Merck, Germany). The solubilized protein was incubated with Ni-NTA agarose beads (Qiagen, Germany) at a ratio of 10 OD_{600} lysate/50 μl bead slurry, rotated at 4 °C for 1 h, and washed extensively to remove non-specific binding. Proteins were eluted with elution buffer (50 mM phosphate buffer pH 8.0, 0.3 M NaCl, 300 mM imidazole, 1 mM PMSF, 1× protease inhibitor cocktail) and subsequently replaced in PBS buffer pH 7.4 (137 mM NaCl, 2.7 mM KCl, 1.8 mM KH_2PO_4 and 10 mM Na_2HPO_4) using desalting column CentriPure 2 - Z25M (emp BIOTECH GmbH, Germany). The purified recombinant rPmKel/GST-6×His and rGST-6×His proteins were analyzed using 10 % SDS-PAGE and confirmed by western blotting with a 1:10,000 dilution of monoclonal anti-His antibody (Abcam, UK).

2.9. Affinity purification/mass spectrometry (AP-MS)

To identify PmKel protein partners in ovary extracts, ~10 OD_{600} lysates of the expressed rPmKel/GST-6×His, rGST-6×His and PBS were immobilized on 50 μl Ni-NTA agarose bead slurry (Qiagen, Germany) in binding buffer (50 mM phosphate buffer pH 8.0, 0.3 M NaCl, 10 % glycerol, 25 mM imidazole). The mixtures were incubated at 4 °C with rotation for 1 h and washed extensively with binding buffer to remove non-specific interactions. Total ovarian proteins were prepared by homogenization in RIPA lysis buffer (50 mM Tris-HCl; pH 7.4, 150 mM NaCl, 1 mM EDTA, 1 % NP-40, 1 % Sodium deoxycholate, 0.1 % SDS, 1× protease inhibitor cocktail) and agitated on ice for 2 h, followed by centrifugation at 13,000 ×*g* for 20 min at 4 °C. The resulting supernatant was collected for subsequent proteomic analysis. For interactome analysis, approximately 1 mg of the ovarian protein extract was added to the purified rPmKel/GST-6×His, GST-6×His, or bead-alone controls, with the reaction volume adjusted to 0.5 ml using binding buffer. The mixtures were incubated at 4 °C with rotation for 2 h, followed by several washes to eliminate non-specific proteins. The bound protein complexes were eluted using elution buffer (50 mM phosphate buffer pH 8.0, 0.3 M NaCl, 300 mM imidazole, 1 mM PMSF). The eluted proteins were analyzed by 10 % SDS-PAGE and subsequently subjected to LC-MS/MS analysis. Identified proteins were searched using Mascot under the SwissProt and NCBI databases, restricted to *Penaeus* taxonomy. Mass tolerances were set at 5 ppm for precursor ions and 0.01 Da for fragment ions. Oxidation of methionine (+15.995 Da) and N-terminal acetylation (+42.011 Da) were set as dynamic modifications, while carbamidomethylation of cysteine (+57.021 Da) was set as a static modification. Proteins identified as Kel-bound were subtracted against proteins bound to GST-6×His and bead alone. Proteins with at least three peptide matches were classified based on functional pathways, with gene ontology (GO) analysis performed using g:Profiler (Reimand et al., 2016) and pathway enrichment using KEGG via ShinyGO 0.81 (Ge, 2020). The Kelch protein interactome in *Drosophila* (Dmel_CG7210) was searched on BioGRID database (Stark, 2006).

2.10. In silico protein complex prediction of PmKel and its partners

Validation of the protein structural folding characteristics of PmKel was carried out using the AlphaFold2 pipeline called ColabFold (Kim et al., 2025). To explore the possible multimeric interaction between PmKel and its potential binding partners, both proteins PmKel (855 aa) and possible interacting proteins; *P. monodon* filamin-A-like (FLNA): 943 aa (XP_037777486.1) and *P. monodon* cleavage and polyadenylation specificity factor subunit 6-like isoform X1 (CPSF): 732 aa (XP_037773525.1), were co-submitted for in silico multimeric formation prediction using AlphaFold2-Multimer v.1 (Evans et al., 2021; Homma et al., 2023) via ColabFold (Kim et al., 2025). The multiple sequence alignment (MSA) was generated via mmseqs2_uniref_env and structural templates were retrieved from the PDB100 database. For the two co-submitted protein pair scenario (PmKel-PmFLNA and PmKel-PmCPSF6-X1), five structural models with 3 recycle attempts each were generated during the prediction. Structural models were colour-coded based on pLDDT scores to visually assess the prediction confidence per residue, following the AlphaFold confidence scheme (Jumper et al., 2021). Functional domains of FLNA and CPSF6 were identified using the SMART database (http://smart.embl-heidelberg.de) and subsequently validated through protein–protein docking with PmKel using HADDOCK 2.4 (Honorato et al., 2021) under default parameters.

2.11. Statistical analysis

All statistical analyses were performed using SPSS 18.0 and GraphPad Prism 8.3.0 softwares. The normality and homogeneity of variances were tested by Kolmogorov–Smirnov and Levene's tests, respectively. Then, the statistically significant differences among treatments ($p < 0.05$) were analyzed by Student's *t*-test or one-way ANOVA followed by Tukey's multiple comparison test.

3. Results

3.1. Validation of the effect of PmEcR silencing on Vg expression

To ensure the effective *PmEcR* silencing and its effects on *Vg* expression in shrimp ovaries, the *EcR*-dsRNA was produced and injected into the shrimp as described in method 2.2. The treatment resulted in a significant knockdown of *PmEcR* (Fig. 1A-C) and two-fold increase in *Vg* expression compared to the control group. Additionally, gonadosomatic index (GSI) was significantly increased in *PmEcR*-silenced shrimp (Fig. 1D). This result confirmed that the samples were suitable for a further study of differential gene expression under *EcR*-knockdown condition.

3.2. Identification of differentially expressed genes in PmEcR-silenced shrimp

To identify *EcR*-responsive genes that probably play roles in vitellogenesis, DEG analysis of *EcR*-silenced shrimp was performed using SSH. High-quality total RNA and efficient subtraction, confirmed by *Actin* amplification, are shown in Fig. S1A-B. Nested PCR revealed distinct patterns between subtracted and un-subtracted groups, especially in the reverse subtraction library (Fig. 2A). Cloned and sequenced bands included genes such as *TSP II*, *Per I*, *uncharacterized LOC 113805388*, *Pole hole-like protein*, *NRAP*, *CDK5 regulatory subunit III*, *GTP-binding protein*, *Kunitz type I*, *ribosomal genes*, *Tryptophan protein 2*, and *non-LTR retrotransposon*. The full list of SSH-identified genes is provided in Table S2. RT-qPCR verification showed that among these genes, only the *uncharacterized LOC113805388* transcript exhibited a strongly significant downregulation in *PmEcR*-silenced samples compared to controls (Fig. 2B).

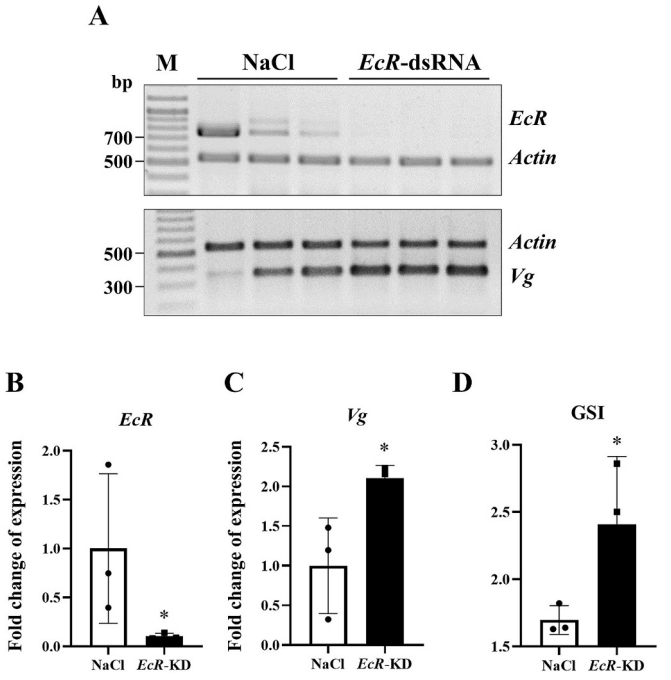

Fig. 1. *EcR* Suppression by *EcR*-dsRNA in ovary.
Mature females *P. monodon* were injected with either 2.5 μg of *EcR*-dsRNA or NaCl (control). The expression levels of *PmEcR* and *Vg* were detected by RT-PCR and analyzed on the same 1.2 % agarose gel as *Actin* that had been amplified in a separate PCR reaction (A). The quantitative fold-changes of *EcR* (B) and *Vg* (C) expression as analyzed by ImageJ ver. 1.54 k were normalized by *Actin* transcript. The GSI values of individual shrimp in each group are calculated and shown as bar graphs (D). An asterisk indicates a statistically significant difference ($p < 0.05$) among groups.

3.3. Structural characterization of uncharacterized LOC 113805388

The cDNA encoding *uncharacterized LOC 113805388* (2568 bp) was obtained via RACE (Fig. S2A). The cDNA sequence was submitted to GenBank (Accession no PQ857654). It encodes an 855-amino acid protein with a theoretical molecular weight of 93 kDa and the pI of 4.83. Both *P. monodon* and *Litopenaeus vannamei* (*L. vannamei*) cDNAs were amplified using ORF-specific primers, PmKel-F and PmKel-R further confirming the transcription of this *locus* (Fig. S2B). AlphaFold-predicted 3D structure analysis of an uncharacterized LOC 113805388 revealed a β-propeller structure formed by six blade-like motifs at the C-terminus, containing Kelch-like domains (Fig. 3A-C; Table S3) and thus, this gene was renamed *PmKel*.

3.4. Ovary-specific expression of PmKel and its inverse correlation with Vg expression

PmKel was exclusively expressed in female shrimp ovaries, with no expression detected in male tissues (Fig. 4A-C, Fig. S3A-B). *PmKel* expression levels were gradually decreased during ovarian development, particularly in stage II ovary, contrasting with the progressive increase in *Vg* expression (Fig. 4D-F). Notably, the declining expression pattern of *PmKel* towards later stages of ovarian development is similar to that of *EcR* (Fig. 4E). These results suggest that *PmKel* and *EcR* may act as a negative regulator of *Vg* expression.

Additionally, to determine whether *PmKel* is actually translated into protein, LC-MS/MS analysis was conducted on *P. monodon*'s ovary proteome. The analysis identified 53 unique peptides out of 271 matched queries that showed strong alignment to PmKel with an overall protein score of 12,751 (Supplementary Document 1). This result confirms that the gene product is expressed at the protein level in ovarian tissue.

3.5. Vg expression was elevated by PmKel silencing

Functional analysis of *PmKel* in *Vg* regulation was performed using RNA interference. *E. coli*-produced long-hairpin dsRNA targeting *PmKel* was obtained (Fig. S4A). The injection of this dsRNA significantly reduced *PmKel* expression in the treated shrimp compared to the controls; NaCl and *GFP*-dsRNA treated groups (Fig. 5A). Consequently, this silencing significantly increased *Vg* expression (Fig. 5B), although the increase in GSI was not statistically significant (Fig. S4B). These findings indicate that *PmKel* negatively regulates *Vg* expression.

3.6. Identification of PmKel protein partners

To investigate the potential function of PmKel in the ovary, its interacting protein partners were identified using affinity purification coupled with mass spectrometry (AP-MS). Recombinant PmKel fused with a GST-6×His tag (rPmKel/GST-6×His, 130 kDa) was produced in *E. coli*. While the rPmKel protein was expressed as an insoluble form, the GST-6×His tag alone was expressed in the soluble fraction with 1 mM IPTG induction (Fig. S5A-B). The rPmKel protein was solubilized using 8 M urea, followed by urea removal and purification using Ni-NTA bead. The purified rPmKel/GST-6×His was eluted with imidazole and confirmed by Coomassie staining and Western blot using an anti-

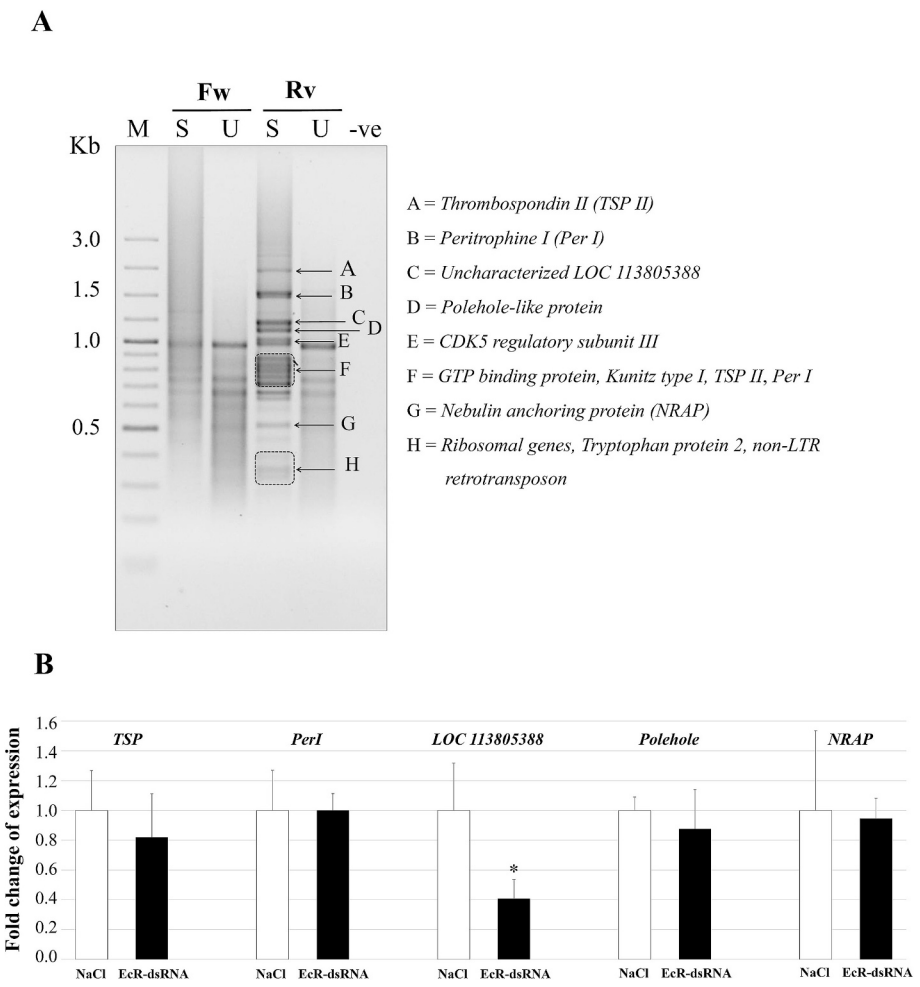

Fig. 2. SSH libraries pattern in *EcR* suppression.
(A) The nested PCR amplification from subtracted (S) and un-subtracted (U) cDNA of forward (Fw) and reverse (Rv) libraries were determined on 1.2 % agarose gel electrophoresis comparing with 100 ng of O'GeneRuler 100 bp Plus DNA Ladder (Thermo Fisher Scientific, USA) in lane M. A negative control reaction containing no DNA template was loaded in lane -ve. The high-intensity different bands from Rv library (down-regulated group) were directly sub-cloned and analyzed by DNA sequencing. The predicted gene for each band as identified by BLAST search is given on the right and indicated by corresponding letter. The expression of these genes, including an uncharacterized *LOC 113805388* was further verified by qPCR using *EF-α* as an internal control (B). The asterisk indicates a statistically significant difference ($p < 0.05$) among groups.

histidine tag antibody (Fig. 6A-B).

Using affinity purification-mass spectrometry (AP-MS) with rPmKel protein, a comprehensive list of 50 potential interacting protein partners was identified, which span diverse biological processes, including gene regulation, nucleosome, and cell division, RNA processing, and metabolism, protein involvement in biogenesis, metabolism, trafficking, transportation, receptor, cytoskeletal, growth factor, cellular metabolism, and of unknown function (Table 2).

Functional annotation through GO analysis revealed enrichment in biological processes such as mRNA metabolic process, cellular component biogenesis, and developmental processes involved in reproduction. The enriched molecular functions included organic cyclic compound binding, mRNA regulatory element binding translation repressor activity, and purine nucleotide binding while cellular component categories highlighted associations with supramolecular complex, ribonucleoprotein complex, and actin cytoskeleton (Fig. 6C). Additionally, KEGG pathway analysis highlighted involvement in dorso-ventral axis formation, RNA degradation, spliceosome, and protein processing in endoplasmic reticulum respectively (Fig. 6D).

3.7. Mapping and dockings of PmKel protein partners in the interactome database

Mapping PmKel protein partners to the *Drosophila melanogaster* Kelch (DmKel) interactome revealed key intersections in cellular processes. A Venn diagram identified two shared interactors, CPSF6 and FLNA, between PmKel and DmKel (Fig. 7A). BioGRID analysis showed direct interactions of DmKel with CPSF6 (CG7185), a cleavage and polyadenylation specificity factor component, and FLNA (CHER), an actin-binding protein involved in cytoskeletal organization. Additionally, DmKel interacts with HTS-KEL, which links to PROSBETA5, a 20S proteasome core subunit (Fig. 7B).

Based on the results of BioGRID analysis in *Drosophila*, possible interactions between PmKel protein and its potential partners, CPSF6 and FLNA in *P. monodon* were further explored. AlphaFold2-Multimer predicted protein-protein complex formation between PmKel and both CPSF6 and FLNA, suggesting possible interaction interfaces. The five structural models generated during the prediction for each complex were shown in Supplementary Document 2. Among them, Model 4 for PmKel-CPSF6 exhibited the best overall confidence (pLDDT = 56.9, pTM = 0.349, ipTM = 0.193; Fig. 7C-D). For PmKel-FLNA complex, Model 5 showed the best overall scores among the candidates (pLDDT =

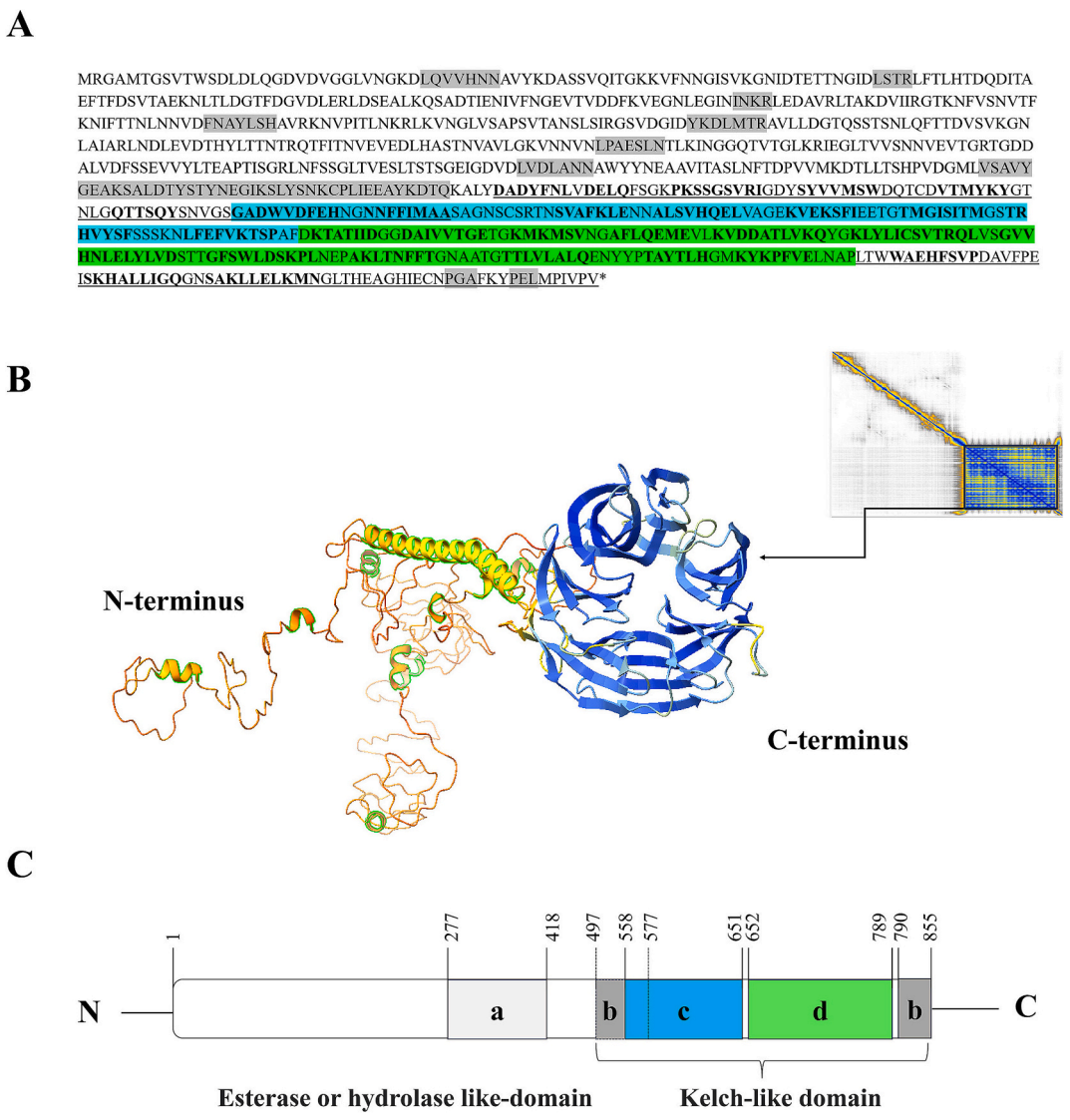

Fig. 3. Structural and functional prediction of an uncharacterized *LOC 113805388* protein.
The deduced amino acid sequence (A), AlphaFold-predicted 3D structure (B), and diagram showing domains predicted by VAST based on 3D structure (C) of uncharacterized *LOC 113805388* were aligned. The grey highlights indicate alpha helix chains, bold residues represent motifs of the β-propeller structure, while underlines, blue, and green highlights indicate the prediction of functional domains by VAST, respectively. In addition, the confident Kelch-like domain prediction by high pLDDT scores (≥90 confirm the structural confidence of the domain) is shown as the blade-like structure at the C-terminus direction in blue (B). (For interpretation of the references to colour in this figure legend, the reader is referred to the web version of this article.)

68.9, pTM = 0.358, ipTM = 0.184; Fig. 7E-F). These values suggest moderate but reliable protein assemblies with satisfactory confidence scores.

To further assess the structural plausibility of these interactions, HADDOCK docking simulations were performed using the β-propeller domain of PmKel and the RS-rich domain of CPSF6 or the calponin homology (CH) domain of FLNA. Docking of PmKel with CPSF6 generated 14 clusters from 119 models, with the top-ranked cluster achieving a *Z*-score of −2.3, and a buried surface area of 2355.1 ± 52.0 Å^2 (Fig. S7A). Similarly, docking with FLNA yielded 12 clusters from 137 models, with a top-ranked cluster exhibiting a Z-score of −1.9, and a buried surface area of 3670.2 ± 539.1 Å^2 (Fig. S7B). These results are consistent with the AlphaFold2-Multimer predictions and further support potential interactions between PmKel and CPSF6 as well as PmKel and FLNA. Taken together, the integration of AlphaFold2-Multimer modeling, docking validation, and evolutionary conservation supports the hypothesis that PmKel engages with CPSF6 and FLNA through protein-protein interfaces.

4. Discussion

Enhancing the reproductive capacity of female shrimp broodstock remains a critical challenge for the shrimp industry. Ovarian development in shrimp is governed by intricate physiological processes, particularly hormonal regulation. In crustaceans, vitellogenesis occurs during the intermolt (resting) stage, a period associated with energy preparation for reproduction (Kang et al., 2014; Wang et al., 2020a, 2020b). Our study reveals that silencing the molting hormone receptor *PmEcR* significantly increases *Vg* expression and GSI, highlighting a negative regulatory role. Although this finding contradicts earlier studies emphasizing the essential role of ecdysteroid signaling on *Vg* expression and ovarian maturation in insects and crustacean (Martín et al., 2001; Parthasarathy et al., 2010; Gong et al., 2015), emerging evidence from several studies offer potential explanations for the observed inhibitory effects of ecdysone on vitellogenin. The ecdysone secreted by the implanted prothoracic glands could inhibit vitellogenin synthesis in the cockroach *Leucophaea maderae* (Engelmann, 2002).

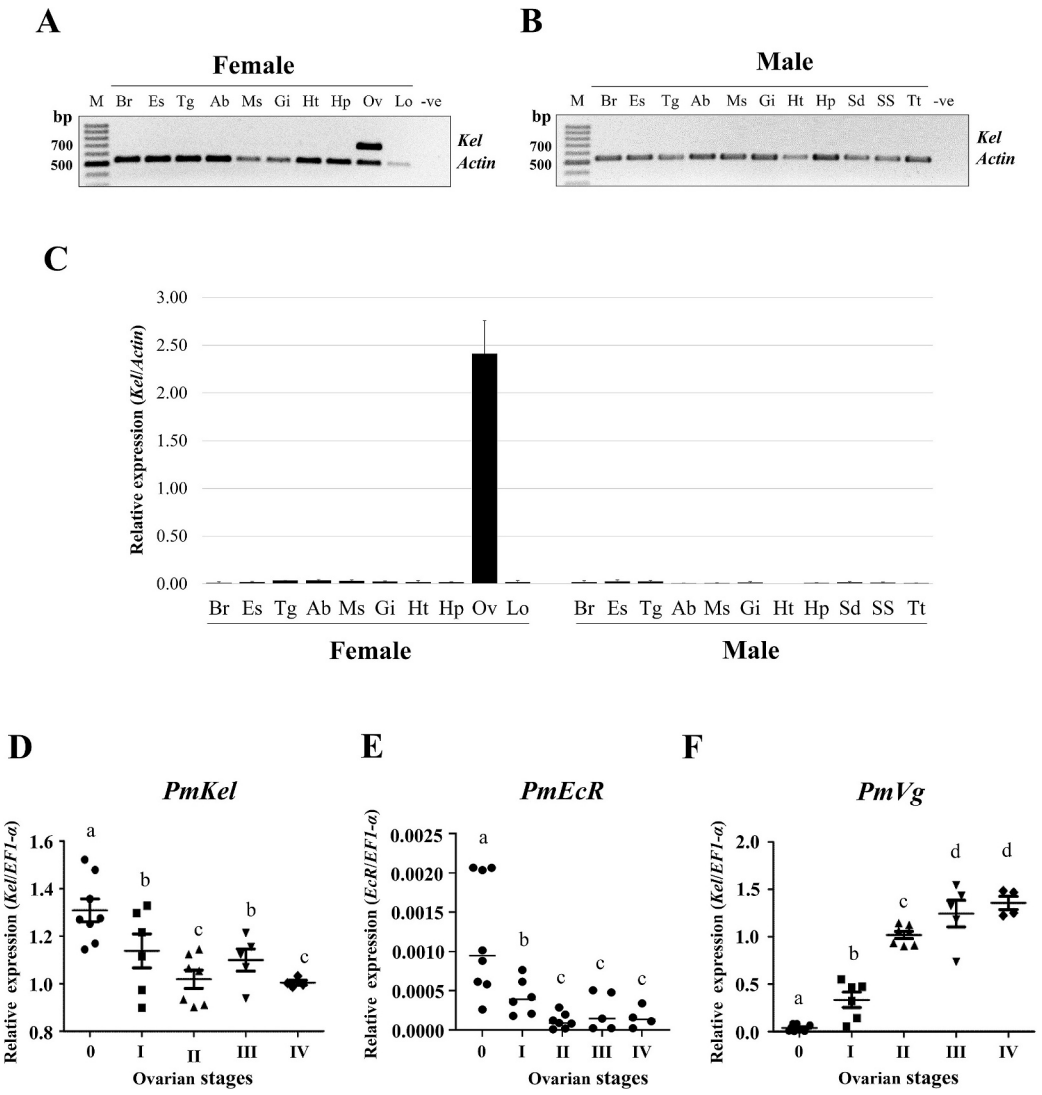

Fig. 4. Expression profile of *PmKel* in shrimp tissues and ovarian developmental stages.
The representative expression profile of *PmKel*, as detected by RT-PCR, shows specific expression in female ovary (A), while no expression was detectable in any tissue of the male shrimp (B). The band intensity of the amplified *PmKel* transcript from tissues including brain (Br), eyestalk (ES), thoracic nerve (Tg), abdominal ganglia (Ab), muscle (Ms), gill (Gi), heart (Ht), hepatopancreas (Hp), lymphoid organ (Ly), ovary (Ov), sperm sac (SS), sperm duct (sd) and testis (TT) of 3 individual shrimp were quantitated using actin transcript as internal control (C). The expression levels of *PmKel* (D), *EcR* (E) and *Vg* (F) in the ovary at each ovarian developmental stage (n = 4–8) were determined by RT-qPCR. The relative amounts of gene transcripts were calculated compared to that of *EF1-α* transcript, and the different letters indicate statistically significant differences at $p < 0.05$.

Similarly, the occurrence of vitellogenin in the pupae of *Apis mellifera* was correlated with low level of ecdysone (Barchuk et al., 2002). In crustacean, a study on the Chinese mitten crab *Eriocheir sinensis* (Su et al., 2020) identified four EcR isoforms in the ovary, with isoforms 3 and 4 showing transcript levels negatively correlated with ecdysteroid titers. This suggests distinct isoform-specific roles in regulating ovarian maturation, possibly including inhibitory effects on *Vg* expression. While only one *EcR* gene has been cloned in *P. monodon* so far, the existence of multiple ovarian *EcR* isoforms cannot be ruled out and warrants further investigation. Additionally, molt suppression may prolong the reproductive cycle. Understanding the underlying mechanisms of these processes requires a deeper knowledge of crustacean biology.

DEG analysis is a powerful approach to uncover gene networks underlying hormonal regulation. In this study, suppression subtractive hybridization (SSH) was used to identify genes responsive to PmEcR silencing. The forward (upregulated) library showed limited signal above background, while the reverse (downregulated) library revealed clearer differential expression patterns. Therefore, we prioritized analysis of the reverse library. Prominent bands were subcloned and sequenced (Fig. 2A), and subsequent RT-qPCR validation identified the *uncharacterized gene LOC113805388* as significantly downregulated, suggesting it may play a key role downstream of *EcR* signaling. Domain analysis of the protein encoded by this gene using Pfam and SMART did not reveal significant matches, but the 3D structural modeling by AlphaFold uncovered a Kelch-like domain as characterized by a β-propeller structure (Fig. 3) Recent advances in 3D structure prediction tools, such as AlphaFold, have been instrumental in annotating uncharacterized proteins and revealing functional insights from predicted structures (Kaur et al., 2023; J. Li et al., 2024). These methods have been beneficial for identifying conserved domains and functional sites in crustacean proteins (Saetang et al., 2022; Hoyos-Gonzalez et al., 2024). The Kelch-like domains are typically involved in protein-protein interactions and regulatory functions (Adams and Kelso, 2000; Prag and Adams, 2003), suggesting that this putative PmKel might have a role in regulating ovarian development. This novel finding lays the foundation for future research into the regulatory pathways governed by PmKel and

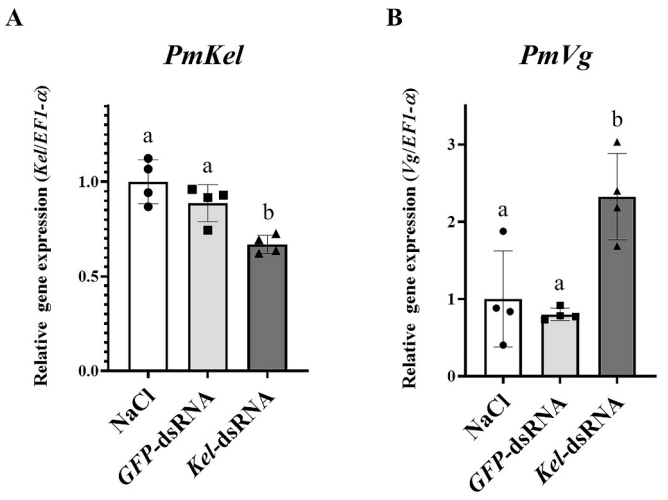

Fig. 5. In vivo *PmKel* Suppression in ovary.
Mature *P. monodon* females were injected with *Kel*-dsRNA at a dose of 2.5 μg. g^{-1} shrimp bw compared to NaCl and *GFP*-dsRNA-treated control (n = 4). At 10 dpi, the expression levels of *PmKel* (A) and *Vg* (B) were determined by RT-qPCR using *EF1-α* transcript as an internal control, and the relative fold changes were normalized to the NaCl-treated group. The different letters indicate statistically significant differences at $p < 0.05$.

its potential significance in *P. monodon* reproduction.

Recent studies in the lepidopteran *Helicoverpa armigera* revealed that BTB and Kelch domain-containing proteins (HaBBP) are upregulated in the fat body and hemocytes during molting and metamorphic stages by 20E. Knockdown of *HaEcR* and *USP* suppressed HaBBP expression, linking Kelch-containing proteins as downstream effectors of the ecdysone pathway (Wang et al., 2011). Similarly, in *Drosophila*, knockdown of the Kelch-containing protein gene (*dKeap1*) reduced ecdysone biosynthetic gene transcription in the prothoracic gland, disrupted ecdysone-regulated early puff gene transcription in salivary glands, and delayed metamorphosis. These findings highlight the critical role of Kelch-containing proteins in regulating ecdysone biosynthesis and downstream gene expression (Chew et al., 2021). Collectively, these studies establish Kelch-containing proteins as central mediators of the ecdysone pathway in arthropod development. In addition, mutations in *Drosophila*'s *Kelch* gene resulted in disorganization of actin in the ring canals, which led to the production of sterile eggs, indicating that the Kelch protein is required for the metamorphosis of ring canals during *Drosophila* oogenesis (Kelso et al., 2002).

Kelch-containing proteins in decapods have been implicated in diverse biological processes, including immunity (Xie et al., 2018; Wang et al., 2020a, 2020b; Yang et al., 2022), antioxidant functions (Huang et al., 2024; Qi et al., 2019; Qiao et al., 2020; Zheng et al., 2022), and sex-biased expression (Xu et al., 2024). In *P. monodon*, 35 kelch-like protein sequences are updated by NCBI genome assembly (GCA_015228065.1). However, these assembled sequences are still uncharacterized by their precise function. The PmKel, a Kelch-like domain-containing protein, discovered in this study exhibits ovary-specific expression, pointing to its specialized role in female reproduction. Although PmKel was detected in ovary proteomic data via LC-MS/MS, further studies are needed to confirm its precise tissue localization, expression dynamics, and functional role. Techniques such as antibody generation and immunodetection will be crucial to deepen our understanding of its involvement in ovarian development.

Notably, *PmKel* expression exhibits an inverse correlation with *Vg* levels during ovarian development, suggesting it may act as a negative regulator of *Vg* expression. Supporting this hypothesis, RNAi-mediated silencing of *PmKel* led to a significant increase in *Vg* expression, reinforcing its putative regulatory role in vitellogenin production. Previous studies in *P. monodon* have shown that ovarian *Vg* expression correlates with vitellin (Vn) protein levels in the ovary during vitellogenesis (Urtgam et al., 2015). This is further evidenced by studies showing that both *GIH* silencing and bursicon-induced *Vg* upregulation eventually led to ovarian development (Treerattrakool et al, 2008; Treerattrakool et al., 2011; Sathapondecha et al., 2015). The data indicate that rising *Vg* expression directly promoted vitellogenin synthesis, leading to vitellin accumulation in the ovary thus, ultimately contributes to ovarian maturation. Together, these results highlight the important role of PmKel as a modulator within reproduction-specific regulatory pathways in crustaceans. However, although an inverse relationship between *PmKel* and *Vg* expression is evident, the current data do not confirm a direct regulatory mechanism, leaving open the possibility of intermediate factors or indirect pathways. Further mechanistic studies, particularly those examining transcriptional regulation and chromatin interactions are necessary to elucidate the exact underlying regulatory mechanisms.

The 3D structure of PmKel features a β-propeller with six blade-like motifs at the C-terminus; the characteristic of Kelch domains that mediate protein-protein interactions. AP-MS analysis identified interactions with several proteins involving in transcriptional regulation, mRNA processing, cytoskeletal organization, and intracellular transport. Guided by the potential interacting proteins of DmKel in *Drosophila*, the possible interactions between PmKel and its candidate partners, CPSF6 and FLNA, were demonstrated through AlphaFold-Multimer, an advanced deep learning tool that reliably predicts the 3D structures of protein complexes with high precision based on the sequences alone (Evans et al., 2021). Additionally, the domain interactions between PmKel and its potential partners, CPSF6 and FLNA, as revealed by Haddock, align well with the protein complex formation predicted by AlphaFold-Multimer. While the results are encouraging, further experimental studies will help solidify the evidence for the formation of these functional complexes.

CPSF6, a component of the cleavage factor Im (CFIm) complex, plays a role in the 3′ end processing of pre-mRNAs. Previous studies have indicated potential roles of mouse CPSF6 during gametogenesis (Noblet and Sartini, 2010; Sartini et al., 2008). In addition, CPSF6 is associated with a nuclear m6A reader YTHDC1 that is required for gonad development in mouse (Kasowitz et al., 2018). Although there is no direct evidence for the role of CPSF6 in ovarian development in crustacean so far, these evidences suggest a possibility that CPSF6 plays its part in precise gene expression during oocyte maturation in the shrimp, probably through the association with PmKel. FLNA is an actin-binding protein that functions to crosslink actin filaments into parallel bundles and thus, contributes to structural integrity and function of cells. Filamin was previously shown to be essential for oogenesis in several species. For example, mammalian FLNA is vital for spindle migration and asymmetric division during oocyte meiosis (Sanjana et al., 2014; Wang et al., 2017). Disrupting filamin in *Drosophila* affected ring canal formation and actin organization leading to impaired oocyte growth and development (Li et al., 1999). Additionally, network analysis linked PmKel to Prosbeta5, a proteasome subunit, suggesting a conserved role in proteasomal regulation required with Kelch to promote the ordered growth of the ring canal cytoskeleton (Hudson et al., 2015; Mannix et al., 2019). These findings establish PmKel as a potential scaffolding protein critical for RNA processing, cytoskeletal organization, and proteasomal function that contributes to ovarian maturation and ecdysteroid-regulated vitellogenesis in *P. monodon*.

In addition, the results suggest potential association of PmKel with epigenetic regulators, including histone H1, H2A.V-like, osa-like Trithorax protein, Y-box factor, and HP1-binding protein. Since these proteins are linked to chromatin remodeling and transcriptional regulation, their association with PmKel suggests that PmKel may modulate *Vg* expression through chromatin-level mechanisms. This points to a potential role for PmKel in epigenetic regulation, possibly downstream of the ecdysone signaling pathway.

Our findings suggest that PmKel may function as a negative regulator

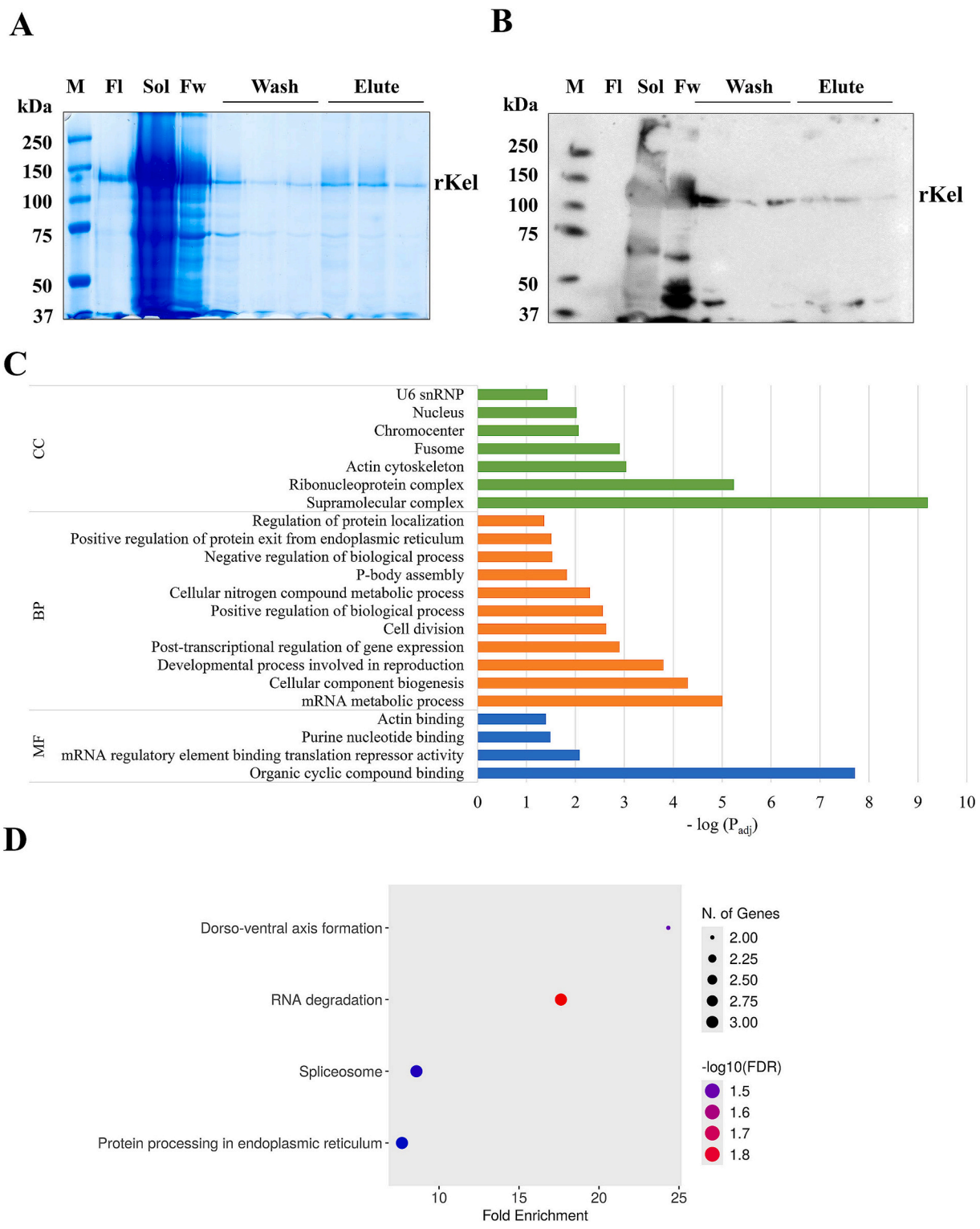

Fig. 6. Identification of PmKel-interacting protein partners by AP-MS.
The purified rKel fused with GST-6×his protein (rPmKel) was analyzed on 10 % SDS-PAGE and stained with Coomassie blue (A). Subsequent verification by western blotting was performed against monoclonal 6×his antibody (B). This purified rPmKel was used as a bait in the affinity purification to determine interacting proteins in the ovarian extract and subsequently subjected to LC-MS/MS. The GO analysis and KEGG enrichment pathways of PmKel interacting protein partners are shown in fig. C and D, respectively. (For interpretation of the references to colour in this figure legend, the reader is referred to the web version of this article.)

of *Vg* expression, providing a basis for further exploration of its role in crustacean reproduction. The PmEcR–Kel axis could represent a potential regulatory pathway contributing to vitellogenesis, and a better understanding of this mechanism may eventually support strategies to improve reproductive performance in shrimp aquaculture. However, as Vg protein levels were not assessed in this study, future work should incorporate proteomic or immunohistochemical approaches to validate these findings at the protein level. Additionally, further experimental validation of the proposed interactions between PmKel and its potential partners, especially CPSF6 and FLNA is necessary to substantiate

Table 2
Identification of interacting partner proteins of Pm-Unc by LC-MS/MS

Protein hit	Symbol	Score(match)	FlyBase ID
Unknown			
Uncharacterized protein LOC113805388	LOC113805388	5351.0 (44)	NA
Uncharacterized protein LOC113821262	LOC113821262	625.0 (10)	NA
Uncharacterized protein LOC113815377	LOC113815377	619.0 (6)	NA
Uncharacterized protein ZK1073.1-like	ZK1073.1	307.0 (5)	NA
Uncharacterized protein LOC113805388	LOC113805388	632.0 (3)	NA
Gene regulation, nucleosome, and cell division			
Y-box factor homolog	YBX1	1545.0 (10)	FBgn0035626
Histone H1	H1	553.0 (8)	FBgn0053834
DNA-binding protein HEXBP-like	HEXBP	459.0 (6)	FBgn0041630
Sex-lethal variant 1	SXL	276.0 (6)	FBgn0264270
Cyclin-dependent serine/threonine-protein kinase	CDK6	220.0 (5)	FBgn0004106
Trithorax group protein osa-like	TRX	197.0 (4)	FBgn0023518
Heterochromatin protein 1-binding protein 3 isoform X8	HP1BP3	199.0 (3)	FBgn0003607
Histone H2A.V-like	H2AV	151.0 (3)	FBgn0001197
RNA processing and metabolism			
Putative ATP-dependent RNA helicase me31b	ME31B	3303.0 (29)	FBgn0004419
Methenyltetrahydrofolate synthase domain-containing protein	MTHFSD	1518.0 (24)	FBgn0263594
Pprotein LSM14 homolog A-like isoform X1	LSM14A	1816.0 (15)	FBgn0041775
rRNA 2'-*O*-methyltransferase fibrillarin-like	FIB2	269.0 (6)	FBgn0003062
LSM3-like	LSM3	398.0 (5)	FBgn0051184
Nucleolar protein-like protein 5 A	NOP56	221.0 (5)	FBgn0038964
Cytoplasmic polyadenylation element-binding protein-like	CPEB2	333.0 (4)	FBgn0264307
Piwi2	PIWI2	303.0 (4)	FBgn0004872
Cleavage and polyadenylation specificity factor subunit 6-like	CPSF6	187.0 (3)	FBgn0035872
U6 snRNA-associated Sm-like protein LSm6	LSM6	129.0 (3)	FBgn0034564
Protein biogenesis and metabolism			
Elongation factor-1 alpha	EEF1A1	393.0 (6)	FBgn0263740
Heterogeneous nuclear ribonucleoprotein L-like	HNRNPLL	183.0 (3)	FBgn0003435
Protein trafficking, trasporter, and receptor			
Glucose-regulated protein 78	GRP78	434.0 (9)	FBgn0001218
Fasciclin-2	FAS2	307.0 (6)	FBgn0000635
Hemocyanin subunit L2	HC	320.0 (5)	FBgn0027657
Hemocyanin subunit L1	HC	172.0 (3)	FBgn0027657
Hrp65 protein	HRP65	138.0 (3)	FBgn0004237
Translocon-associated protein subunit gamma-like	SSR1	133.0 (3)	FBgn0025700
Structural protein			
Myosin heavy chain	MYH1	1405.0 (21)	FBgn0264695
Beta-actin	ACTB	764.0 (12)	FBgn0011743
Cytoplasmic-type actin 3	ACT3	634.0 (10)	FBgn0011743
Actin 1	ACT1	480.0 (8)	FBgn0011743
Lamin Dm0	LAM	364.0 (7)	FBgn0002525
Tubulin beta-1 chain	TUBB1	490.0 (6)	FBgn0284243
Tropomyosin isoform	TPM	313.0 (6)	FBgn0003721
Myosin essential light chain	MLCE	353.0 (4)	FBgn0002772
Filamin-A-like	FLNA	230.0 (4)	FBgn0014141
Leucine rich repeat only protein 1	LRRC1	224.0 (4)	FBgn0036924
Titin	TTN	187.0 (4)	FBgn0086906
Tropomyosin-like	TPM	223.0 (3)	FBgn0003721
Lamin Dm0	LAM	215.0 (3)	FBgn0002525
Spectrin alpha chain	SPTA1	185.0 (3)	FBgn0250789
Growth factor			
Putative insulin-like growth factor 2 mRNA-binding protein 1	IGF2BP3	375.0 (7)	FBgn0285926
Cellular metabolism			
Sodium/potassium-transporting ATPase subunit alpha	ATP1A1	755.0 (13)	FBgn0267363
Glyceraldehyde 3-phosphate dehydrogenase	GAPDH	204.0 (3)	FBgn0001091
Methylcrotonoyl-CoA carboxylase beta chain	MCCB	197.0 (3)	FBgn0042083
GTP-binding protein SAR1B	SAR1B	175.0 (3)	FBgn0038947
F1-ATP synthase beta subunit	ATP5F1B	147.0 (3)	FBgn0010217

functional relevance of these protein complexes. Together, these will help elucidate the molecular mechanisms underlying PmKel function and its possible interactions with other regulatory pathways. Additionally, the ability to clone PmKel in the ovary of *L. vannamei* (Fig. S2B) may offer valuable insights for other economically significant crustaceans.

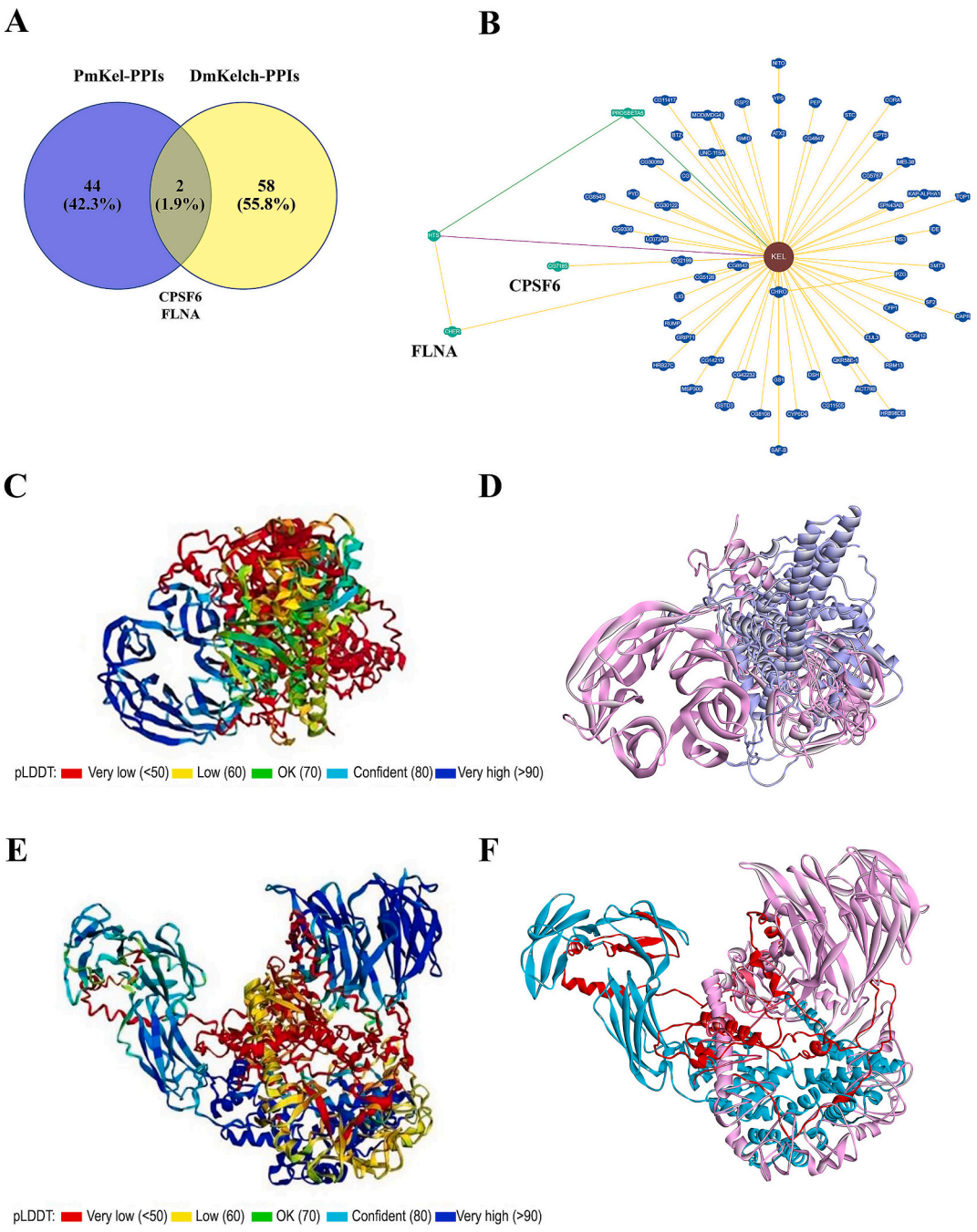

Fig. 7. In silico protein complex prediction of PmKel protein partners.
(A) Venn diagram showing two overlapping proteins, CPSF6 and FLNA, shared between PmKel interactors and the *Drosophila* Kelch (DmKel) interactome. (B) Interaction network from the BioGRID database illustrating direct interactions of DmKel with CPSF6 (CG7185) and FLNA (CHER), along with associated nodes including KEL, HTS-KEL, and the proteasome subunit PROSBETA5. (C) AlphaFold-Multimer Model 4 of the PmKel and PmCPSF6 complex coloured by per residue confidence score: high-confidence regions are shown in blue, moderate in green, and low-confidence or disordered regions in red (pLDDT = 56.9). (D) AlphaFold-Multimer Model 4 of PmKel (855 aa, pink) and PmCPSF6 (732 aa, purple), showing predicted interface interaction when coloured by protein identity. (E) Model 5 of PmKel and PmFLNA complex from AlphaFold Multimer with good overall confidence scores (pLDDT = 68.9). (F) In AlphaFold Multimer Model 5, the core structure of PmKel (residues 115–855, pink) and the N-terminal portion of the partner PmFLNA (residues 1–599, cyan) form a compact protein assembly. The N-terminal region (residues 1–114) of PmKel and C-terminal segment (residues 600–943) of PmFLNA are predicted to be unstructured (red), but the rest of this complex exhibits satisfactory pLDDT scores. (For interpretation of the references to colour in this figure legend, the reader is referred to the web version of this article.)

5. Conclusion

This study highlights a critical role of the ecdysteriod signaling pathway in regulating vitellogenin synthesis in *P. monodon*. In addition, through structural and function analyses of a potential down-regulated gene upon *EcR*-knockdown, PmKel was identified as a key player in shrimp reproduction, acting downstream of PmEcR to negatively regulate vitellogenin expression. While further verification is required, these findings contribute to a growing understanding of the molecular mechanisms underlying ovarian development in crustaceans and may offer molecular basis for developing reproductive management strategies in aquaculture.

CRediT authorship contribution statement

Jakkapong Kluebsoongnoen: Conceptualization, Methodology, Investigation, Visualization, Formal analysis, Writing – original draft. **Duangrudee Tanramluk**: Methodology, Visualization, Formal analysis, Writing – review & editing. **Maryam Jozghorbani**: Methodology. **Jutarop Phetcharaburanin**: Writing – review & editing. **Tomasz J. Sarnowski**: Supervision, Formal analysis, Writing – review & editing. **Apinunt Udomkit**: Conceptualization, Formal analysis, Supervision, Writing – review & editing, Funding acquisition.

Funding resources

This work was financially supported by the National Research Council of Thailand (NRCT) and Mahidol University (NRCT5-RSA63015-04), the human resource funding support from the NSRF via the Program Management Unit for Human Resources & Institutional Development, Research and Innovation (grant No. B13F680068), and TJS was supported by the National Science Center, Poland (NCN) grant No. UMO-2018/30/M/NZ1/00180.

Declaration of competing interest

The authors declare that they have no known competing financial interests or personal relationships that could have appeared to influence the work reported in this paper.

Acknowledgements

We sincerely thank Mr. Vichai Boonsai for providing shrimp samples, Ms. Chawewan Chimwai, Ms. Pannee Thongboonsong, Ms. Orathai Namramoon, Ms. Apisara Saensuwanna, Dr. Jaroslaw Steciuk, Dr. Paulina Oksinska and Dr. Thaneeya Nantapojd for technical assistance. The equipment used was sponsored in part by the Centre for Preclinical Research and Technology (CePT), a project co-sponsored by European Regional Development Fund and Innovative Economy, The National Cohesion Strategy of Poland.

Appendix A. Supplementary data

Supplementary data to this article can be found online at https://doi.org/10.1016/j.cbpa.2025.111914.

Data availability

Data will be made available on request.

References

Adams, J., Kelso, R., 2000. The kelch repeat superfamily of proteins: propellers of cell function. Trends Cell Biol. 10 (1), 17–24. https://doi.org/10.1016/s0962-8924(99)01673-6.

Barchuk, A.R., Bitondi, M.M., Simões, Z.L., 2002. Effects of juvenile hormone and ecdysone on the timing of vitellogenin appearance in hemolymph of queen and worker pupae of Apis mellifera. J. Insect Sci. 2, 1–8. https://doi.org/10.1673/031.002.0101.

Chew, L.Y., Zhang, H., He, J., Yu, F., 2021. The Nrf2-Keap1 pathway is activated by steroid hormone signaling to govern neuronal remodeling. Cell Rep. 36 (5), 109466. https://doi.org/10.1016/j.celrep.2021.109466.

Costantino, B.F.B., Bricker, D.K., Alexandre, K., Shen, K., Merriam, J.R., Antoniewski, C., et al., 2008. A novel ecdysone receptor mediates steroid-regulated developmental events during the mid-third instar of *Drosophila*. PLoS Genet. 4 (6), e1000102. https://doi.org/10.1371/journal.pgen.1000102.

Ding, S., Huang, M., Sheng, N., Chen, T., Xu, R., Luo, Z., Huang, X., Wan, Z., Su, S., Li, X., 2023. RNAi-mediated knockdown of the mandibular organ-inhibiting hormone (*MOIH*) gene stimulates vitellogenesis in the Chinese mitten crab *Eriocheir sinensis*. Fish. Sci. 89, 399–408. https://doi.org/10.1007/s12562-023-01680-y.

Engelmann, F., 2002. Ecdysteroids, juvenile hormone and vitellogenesis in the cockroach *Leucophaea maderae*. J. Insect Sci. 2 (1), 20. https://doi.org/10.1093/jis/2.1.20.

Evans, R., O'Neill, M., Pritzel, A., Antropova, N., Senior, A., Green, T., Žídek, A., Bates, R., Blackwell, S., Yim, J., Ronneberger, O., Bodenstein, S., Zielinski, M., Bridgland, A., Potapenko, A., Cowie, A., Tunyasuvunakool, K., Jain, R., Clancy, E., Kohli, P., Jumper, J., Hassabis, D., 2021. Protein complex prediction with AlphaFold-Multimer. bioRxiv. https://doi.org/10.1101/2021.10.04.463034, 10.04.463034.

Ge, S.X., 2020. ShinyGO: a graphical gene-set enrichment tool for animals and plants. Bioinformatics 15;36 (8), 2628–2629. https://doi.org/10.1101/082511.Lai.

Gong, J., Ye, H., Xie, Y., Yang, Y., Huang, H., Li, S., Zeng, C., 2015. Ecdysone receptor in the mud crab *Scylla paramamosain*: a possible role in promoting ovarian development. J. Endocrinol. 224 (3). https://doi.org/10.1530/JOE-14-0526.

Gong, J., Huang, C., Shu, L., Bao, C., Huang, H., Ye, H., Zeng, C., Li, S., 2016. The retinoid X receptor from mud crab: new insights into its roles in ovarian development and related signaling pathway. Sci. Rep. 6 (1), 23654. https://doi.org/10.1038/srep23654.

Homma, F., Huang, J., van der Hoorn, R.A.L., 2023. AlphaFold-Multimer predicts cross-kingdom interactions at the plant-pathogen interface. Nat. Commun. 14 (1), 6040. https://doi.org/10.1038/s41467-023-41721-9.

Honorato, R.V., Koukos, P.I., Jiménez-García, B., Tsaregorodtsev, A., Verlato, M., Giachetti, A., Rosato, A., Bonvin, A.M.J.J., 2021. Structural biology in the clouds: the WeNMR-EOSC ecosystem. Front. Mol. Biosci. 28 (8), 729513. https://doi.org/10.3389/fmolb.2021.729513.

Hoyos-Gonzalez, N., Ochoa-Leyva, A., Benitez-Cardoza, C.G., Brieba, L.G., Lukaszewicz, G., Trasviña-Arenas, C.H., Sotelo-Mundo, R.R., 2024. Identification of a cryptic functional apolipophorin-III domain within the Prominin-1 gene of *Litopenaeus vannamei*. Comp. Biochem. Physiol. B Biochem. Mol. Biol. 270, 1109280. https://doi.org/10.1016/j.cbpb.2023.110928.

Huang, P., Gao, J., Du, J., Nie, Z., Li, Q., Sun, Y., Xu, G., Cao, L., 2024. Prometryn exposure disrupts the intestinal health of *Eriocheir sinensis*: physiological responses and underlying mechanism. Comp Biochem Physiol C Toxicol Pharmacol. 277, 109820. https://doi.org/10.1016/j.cbpc.2023.109820.

Hudson, A.M., Mannix, K.M., Cooley, L., 2015. Actin cytoskeletal organization in drosophila germline ring canals depends on kelch function in a Cullin-RING E3 ligase. Genetics 201 (3), 1117–1131. https://doi.org/10.1534/genetics.115.181289.

Jumper, J., Evans, R., Pritzel, A., Green, T., Figurnov, M., Ronneberger, O., Tunyasuvunakool, K., Bates, R., Žídek, A., Potapenko, A., Bridgland, A., Meyer, C., Kohl, S.A.A., Ballard, A.J., Cowie, A., Romera-Paredes, B., Nikolov, S., Jain, R., Adler, J., Hassabis, D., 2021. Highly accurate protein structure prediction with AlphaFold. Nature 596 (7873), 583–589. https://doi.org/10.1038/s41586-021-03819-2.

Kang, B.J., Okutsu, T., Tsutsui, N., Shinji, J., Bae, S.H., Wilder, M.N., 2014. Dynamics of vitellogenin and vitellogenesis-inhibiting hormone levels in adult and subadult whiteleg shrimp, *Litopenaeus vannamei*: relation to molting and eyestalk ablation. Biol. Reprod. 90 (1), 12. https://doi.org/10.1095/biolreprod.113.112243.

Kasowitz, S.D., Ma, J., Anderson, S.J., Leu, N.A., Xu, Y., Gregory, B.D., et al., 2018. Nuclear m6A reader YTHDC1 regulates alternative polyadenylation and splicing during mouse oocyte development. PLoS Genet. 14 (5), e1007412. https://doi.org/10.1371/journal.pgen.1007412.

Kaur, G., Ren, R., Hammel, M., Horton, J.R., Yang, J., Cao, Y., He, C., Lan, F., Lan, X., Blobel, G.A., Blumenthal, R.M., Zhang, X., Cheng, X., 2023. Allosteric autoregulation of DNA binding via a DNA-mimicking protein domain: a biophysical study of ZNF410-DNA interaction using small angle X-ray scattering. Nucleic Acids Res. 51 (4), 1674–1686. https://doi.org/10.1093/nar/gkac1274.

Kelso, R.J., Hudson, A.M., Cooley, L., 2002. Drosophila Kelch regulates actin organization via Src64-dependent tyrosine phosphorylation. J. Cell Biol. 156 (4), 703–713. https://doi.org/10.1083/jcb.200110063.

Kim, G., Lee, S., Levy, K.E., Kim, H., Moriwaki, Y., Ovchinnikov, S., et al., 2025. Easy and accurate protein structure prediction using ColabFold. Nat. Protoc. 20 (3), 620–642. https://doi.org/10.1038/s41596-024-01060-5.

Kluebsoongnoen, J., Panyim, S., Sarnowski, T.J., Udomkit, A., 2021. Retinoid X receptor modulates vitellogenin gene expression in black tiger shrimp, *Penaeus monodon*. Comp. Biochem. Physiol. A Mol. Integr. Physiol. 254, 110877. https://doi.org/10.1016/j.cbpa.2020.110877.

Kluebsoongnoen, J., Saensuwanna, A., Jozghorbani, M., Ho, T., Szolajska, E., Sarnowski, T., Udomkit, A., 2023. A possible role of the ecdysone receptor in modulating gonad-inhibiting hormone gene expression in the black tiger prawn, *Penaeus monodon*. Aquaculture 569, 739393. https://doi.org/10.1016/j.aquaculture.2023.739393.

Li, M.-G., Serr, M., Edwards, K., Ludmann, S., Yamamoto, D., Tilney, L.G., Field, C.M., Hays, T.S., 1999. Filamin is required for ring canal assembly and actin organization during Drosophila oogenesis. J. Cell Biol. 146 (5), 1061–1074. https://doi.org/10.1083/jcb.146.5.1061.

Li, J., Mui, J.W.Y., da Silva, B.M., Pires, D.E.V., Ascher, D.B., Madiedo Soler, N., Goddard-Borger, E.D., Williams, S.J., 2024. A broad-spectrum α-glucosidase of glycoside hydrolase family 13 from *Marinovum sp.*, a member of the Roseobacter clade. Appl. Biochem. Biotechnol. 196 (9), 6059–6071. https://doi.org/10.1007/s12010-023-04820-3.

Livak, K.J., Schmittgen, T.D., 2001. Analysis of relative gene expression data using real-time quantitative PCR and the $2^{-\Delta\Delta CT}$ method. Methods 25 (4), 402–408. https://doi.org/10.1006/meth.2001.1262.

Lu, Y., Liu, M., Gong, J., Cheng, Y., Wu, X., 2018. Effect of exogenous estrogen on the ovarian development and gene expression in the female swimming crab *Portunus trituberculatus* (Miers, 1876) (Decapoda: Brachyura: Portunidae). J. Crustac. Biol. 38 (3), 367–373. https://doi.org/10.1093/jcbiol/ruy013.

Mannix, K.M., Starble, R.M., Kaufman, R.S., Cooley, L., 2019. Proximity labeling reveals novel interactomes in live Drosophila tissue. Development 146 (14), 176644. https://doi.org/10.1242/DEV.176644.

Martín, D., Wang, S.F., Raikhel, A.S., 2001. The vitellogenin gene of the mosquito *Aedes aegypti* is a direct target of ecdysteroid receptor. Mol. Cell. Endocrinol. 173 (1–2), 75–86. https://doi.org/10.1016/S0303-7207(00)00413-5.

Nagaraju, G.P.C., 2011. Reproductive regulators in decapod crustaceans: an overview. J. Exp. Biol. 214 (Pt 1), 3–16. https://doi.org/10.1242/jeb.047183.

Noblet, E., Sartini, B.L., 2010. Developmental characterization of cleavage factor im (CFIm) polyadenylation factor during oogenesis. Biol. Reprod. 83 (Suppl_1), 413. https://doi.org/10.1093/biolreprod/83.s1.413.

Parthasarathy, R., Sheng, Z., Sun, Z., Palli, S.R., 2010. Ecdysteroid regulation of ovarian growth and oocyte maturation in the red flour beetle, *Tribolium castaneum*. Insect Biochem. Mol. Biol. 40 (6), 429–439. https://doi.org/10.1016/j.ibmb.2010.04.002.

Pettersen, E.F., Goddard, T.D., Huang, C.C., Meng, E.C., Couch, G.S., Croll, T.I., Morris, J. H., Ferrin, T.E., 2021. UCSF ChimeraX : structure visualization for researchers, educators, and developers. Protein Sci. 30 (1), 70–82. https://doi.org/10.1002/pro.3943.

Prag, S., Adams, J.C., 2003. Molecular phylogeny of the kelch-repeat superfamily reveals an expansion of BTB/kelch proteins in animals. BMC Bioinformatics. 4, 42. https://doi.org/10.1186/1471-2105-4-42.

Qi, C., Wang, X., Han, F., Jia, Y., Lin, Z., Wang, C., Lu, J., Yang, L., Wang, X., Li, E., Qin, J.G., Chen, L., 2019. Arginine supplementation improves growth, antioxidant capacity, immunity, and disease resistance of juvenile Chinese mitten crab, *Eriocheir sinensis*. Fish Shellfish Immunol. 93, 463–473. https://doi.org/10.1016/j.fsi.2019.07.082.

Qiao, X., Liang, Q., Liu, Y., Wang, W., 2020. A novel Kelch-like-1 is involved in antioxidant response by regulating antioxidant enzyme system in *Penaeus vannamei*. Genes (Basel) 11 (9), 1077. https://doi.org/10.3390/genes11091077.

Reimand, J., Arak, T., Adler, P., Kolberg, L., Reisberg, S., Peterson, H., Vilo, J., 2016. G: profiler—a web server for functional interpretation of gene lists (2016 update). Nucleic Acids Res. 44 (W1), W83–W89. https://doi.org/10.1093/nar/gkw199.

Saetang, J., Tipmanee, V., Benjakul, S., 2022. *In silico* prediction of cross-reactive epitopes of tropomyosin from shrimp and other arthropods involved in allergy. Molecules 27 (9), 2667. https://doi.org/10.3390/molecules27092667.

Sanjana, N.E., Shalem, O., Zhang, F., 2014. Improved vectors and genome-wide libraries for CRISPR screening. Nat. Methods 11, 783–784. https://doi.org/10.1038/nmeth.3047.

Sartini, B.L., Wang, H., Wang, W., Millette, C.F., Kilpatrick, D.L., 2008. Pre-messenger RNA cleavage factor I (CFIm): potential role in alternative polyadenylation during spermatogenesis. Biol. Reprod. 78 (3), 472–482. https://doi.org/10.1095/biolreprod.107.064774.

Sathapondecha, P., Panyim, S., Udomkit, A., 2015. A novel function of bursicon in stimulation of vitellogenin expression in black tiger shrimp, *Penaeus monodon*. Aquaculture 446, 80–87. https://doi.org/10.1016/j.aquaculture.2015.04.027.

Schneider, C.A., Rasband, W.S., Eliceiri, K.W., 2012. NIH image to ImageJ: 25 years of image analysis. Nat. Methods 9, 671–675. https://doi.org/10.1038/nmeth.2089.

Stark, C., 2006. BioGRID: a general repository for interaction datasets. Nucleic Acids Res. 34, 535–539. https://doi.org/10.1093/nar/gkj109.

Su, Y., Guo, Q., Gong, J., Cheng, Y., Wu, X., 2020 Oct. Functional expression patterns of four ecdysteroid receptor isoforms indicate their different functions during vitellogenesis of Chinese mitten crab, *Eriocheir sinensis*. Comp. Biochem. Physiol. A Mol. Integr. Physiol. 248. https://doi.org/10.1016/j.cbpa.2020, 110754.

Subramoniam, T., 2000. Crustacean ecdysteriods in reproduction and embryogenesis. Comp Biochem Physiol C Toxicol Pharmacol. 125 (2), 135–156. https://doi.org/10.1016/S0742-8413(99)00098-5.

Tan-fermin, J.D., Pudadera, R.A., 1989. Ovarian maturation stages of the wild Giant Tiger prawn, *Penaeus monodon*. Fabricius. Aquaculture. 77 (2–3), 229–242. https://doi.org/10.1016/0044-8486(89)90205-6.

Treerattrakool, s., Panyim, S., Udomkit, A., 2011. Induction of ovarian maturation and spawning in *Penaeus monodon* broodstock by double-stranded RNA. Mar. Biotechnol. 13 (2), 163–169. https://doi.org/10.1007/s10126-010-9276-0.

Treerattrakool, S., Panyim, S., Chan, S.M., Withyachumnarnkul, B., Udomkit, A., 2008. Molecular characterization of gonad-inhibiting hormone of *Penaeus monodon* and elucidation of its inhibitory role in vitellogenin expression by RNA interference. FEBS J. 275 (5), 970–980. https://doi.org/10.1111/j.1742-4658.2008.06266.x.

Tsukimura, B., 2001. Crustacean vitellogenesis: its role in oocyte development1. Am. Zool. 41 (3), 465–476. https://doi.org/10.1093/icb/41.3.465.

Urtgam, S., Treerattrakool, S., Roytrakul, S., Wongtripop, S., Prommoon, J., Panyim, S., Udomkit, A., 2015. Correlation between gonad-inhibiting hormone and vitellogenin during ovarian maturation in the domesticated *Penaeus monodon*. Aquaculture 437, 1–9. https://doi.org/10.1016/j.aquaculture.2014.11.014.

Wang, G., Liu, P.C., Wang, J.X., Zhao, X.F., 2011. A BTB domain-containing gene is upregulated by immune challenge. Arch. Insect Biochem. Physiol. 77 (2), 58–71. https://doi.org/10.1002/arch.20421.

Wang, H., Guo, J., Lin, Z., Namgoong, S., Oh, J.S., Kim, N.-H., 2017. Filamin A is required for spindle migration and asymmetric division in mouse oocytes. FASEB J. 31, 3677–3688. https://doi.org/10.1096/fj.201700056R.

Wang, W., Li, B., Zhou, T., Wang, C., Kyei, A.B., Shi, L., Chan, S., 2020a. Investigation of gene sequence divergence, expression dynamics, and endocrine regulation of the vitellogenin gene family in the whiteleg shrimp *Litopenaeus vannamei*. Front Endocrinol (Lausanne). 11, 577745. https://doi.org/10.3389/fendo.2020.577745.

Wang, C., Wang, X., Huang, Y., Bu, X., Xiao, S., Qin, C., Qiao, F., Qin, J.G., Chen, L., 2020b. Effects of dietary T-2 toxin on gut health and gut microbiota composition of the juvenile Chinese mitten crab (*Eriocheir sinensis*). Fish Shellfish Immunol. 106, 574–582. https://doi.org/10.1016/j.fsi.2020.08.019.

Webster, S.G., Keller, R., Dircksen, H., 2012. The CHH-superfamily of multifunctional peptide hormones controlling crustacean metabolism, osmoregulation, moulting, and reproduction. Gen. Comp. Endocrinol. 175 (2), 217–233. https://doi.org/10.1016/j.ygcen.2011.11.035.

Xie, X., Chang, X., Gao, Y., Li, D., Liu, L., Liu, M., 2018. An Ns1abp-like gene promotes white spot syndrome virus infection by interacting with the viral envelope protein VP28 in red claw cray fi sh *Cherax quadricarinatus*. Dev. Comp. Immunol. 84, 264–272. https://doi.org/10.1016/j.dci.2018.03.001.

Xu, Y., Yu, F., Feng, W., Wei, J., Su, S., Li, J., Hua, G., Li, W., Tang, Y., 2024. Genetic variation mining of the Chinese mitten crab (*Eriocheir sinensis*) based on transcriptome data from public databases. Brief. Funct. Genomics 23 (6), 816–827. https://doi.org/10.1093/bfgp/elae030.

Yang, L., Wang, Z., Geng, R., Niu, S., Zuo, H., 2022. A kelch motif-containing protein KLHDC2 regulates immune responses against *Vibrio parahaemolyticus* and white spot syndrome virus in *Penaeus vannamei*. Fish Shellfish Immunol. 127, 187–194. https://doi.org/10.1016/j.fsi.2022.06.009.

Zheng, N., Wang, N., Wang, Z., Yu, Abdallah, Zhang, G., Yuan, B., Wang, S., Yao, Q., Chen, Y., Wang, Ke, Ju, Q., Zhang, D. Ming, 2022. Effect of infection with *Aeromonas hydrophila* on antioxidant capacity, inflammation response, and apoptosis proteins in Chinese mitten crab (*Eriocheir sinensis*). Comp Biochem Physiol C Toxicol Pharmacol. 252, 109220. https://doi.org/10.1016/j.cbpc.2021.109220.

Zmora, N., Trant, J., Zohar, Y., Chung, J.S., 2009. Molt-inhibiting hormone stimulates vitellogenesis at advanced ovarian developmental stages in the female blue crab, *Callinectes sapidus* 1: an ovarian stage dependent involvement. Saline Syst. 5, 7. https://doi.org/10.1186/1746-1448-5-7.